AIAA AVIATION Forum
June 25-29, 2018, Atlanta, Georgia
2018 Atmospheric and Space Environments Conference

10.2514/6.2018-3830

Aerodynamic, Laser Scanning and Photogrammetric Measurements of Cold Soaked Fuel Frost

Erkki Soinne[1]
Finnish Transport Safety Agency, Helsinki, FI-00101, Finland

Tomi Rosnell[2]
Finnish Geospatial Research Institute of National Land Survey, Helsinki, FI-00521, Finland

After an aircraft landing during a stopover Cold Soaked Fuel Frost is often formed on the wing even at temperatures above 0° C. It is of interest to measure the frost geometry and corresponding aerodynamic effect on lift coefficient. To investigate these effects a HL-CRM wing model, representing the wing of a modern jet aircraft, was built including a wing tank cooling system. Real frost was generated on the wing in a wind tunnel test section and the frost thickness was measured with an Elcometer gauge. Frost surface geometry was measured with laser scanning and photogrammetry. The measurements were made with titanium dioxide painting to enhance surface reflectivity and without painting. The accuracy of laser scanning and photogrammetry were compared in these four cases. The aerodynamic effect of the frost was studied in a simulated aircraft take-off sequence, in which the speed was accelerated to a typical rotation speed and the wing model was then rotated to an angle of attack used at initial climb. Time histories of the lift coefficient were measured with a force balance. Time histories of the upper surface boundary layer displacement thickness were measured with a boundary layer rake. The measurements showed that depending on the ambient temperature the frost may evaporate/melt during the take-off sequence. Highest lift losses occurred after the rotation. The lift losses correlated with average frost thickness and the increase of the boundary layer displacement thickness.

Nomenclature

c	=	wing model chord
C_L	=	wing lift coefficient
C_{LClean}	=	clean wing lift coefficient
t	=	frost thickness
U	=	wind tunnel velocity
V_R	=	rotation speed
V_2	=	take-off safety speed
α	=	angle of attack
δ^*	=	boundary layer displacement thickness

I. Introduction

Cold Soaked Fuel Frost (CSFF) is formed on aircraft wing tank area on ground when the aircraft has been at high altitude where the wing structure and fuel have been cooled down. Frost formation depends on ambient temperature, humidity and other factors such as wind speed causing forced convection. A literature review on CSFF formation is presented by Koivisto in Ref. [1]. The phenomenon is known by aircraft manufacturers, airlines and the authorities, but there are only a few publications with real frost related to aircraft. Ljungsröm performed in Ref. [2] wind tunnel tests on NACA 65_2-A215 airfoil with abrasive paper to simulate the effect of hoar frost in representative take-off configurations with and without a flap and slat. Oolbekkink and Volkers made in Ref. [3] wind tunnel tests and on NACA 63_2-015 airfoil with sandpaper as well as theoretical calculations to simulate the effect of frost.

[1] Chief Adviser Aeronautics, Organization Services Department, Member AIAA.
[2] Research Scientist, Department of Remote Sensing and Photogrammetry

Artificial copies of real frost were made in Ref. [4] by Kind and Lawrysyn and tested in wind tunnel on a flat plate to investigate the effect of frost on the boundary layer. According to Bragg et al in Ref. [5] frost on an airfoil lower surface, simulated with distributed roughness particles, is significant only when it exists far enough forward to affect the upper surface boundary layer. Effects of CSFF have been studied by Koivisto in Refs. [6] and [7] using a cooled wind tunnel model and real frost on two generic jet aircraft wing airfoils, the Boeing designed HL-CRM and an Airbus type DLR-F15 airfoil.

Cold Soaked Fuel Frost is of interest for the next take-off after a stopover. Traditionally the Federal Aviation Administration of the United States has required in the operative regulation of Ref. [8] paragraph 121.629(b) that "No person may take off an aircraft when frost, ice, or snow is adhering to the wings…Takeoffs with frost under the wing in the area of fuel tanks may be authorized by the Administrator". In other words a clean wing concept has been required on the upper wing surface. The European Aviation Safety Agency has a different approach in the operative regulation of Ref. [9] paragraph CAT.OP.MPA.250(b), where it says that "The commander shall only commence take-off if the aircraft is clear of any deposit that might adversely affect the performance or controllability of the aircraft". So EASA allows contamination when it does not adversely affect operation of the aircraft. Transport Canada allows contamination on the wing in take-off in the same way as EASA, provided that there is no adverse effect. At present there is an EASA and Transport Canada approval for the Boeing 737NG aircraft to perform a take-off with certain amount of CSFF on the wing upper side. The FAA has also given an exemption for this aircraft.

The FAA and the Finnish Transport Safety Agency Trafi have a Research Agreement on aircraft icing research with an emphasis on ground icing such as the effects of anti-icing fluids and CSFF. The present investigation is part of this research agreement. It is focused on wind tunnel tests of a wing model with real cold soaked fuel frost. The wing model has a wing tank with surrogate fuel to cool the model for frost generation. A simulated take-off was performed by first accelerating the wind tunnel flow to simulate aircraft take-off roll on the ground with the wing at zero angle of attack. Then the model was rotated to an angle of attack α representing initial climb. Time histories of the wing model lift coefficient and upper surface boundary layer displacement thickness were measured during the take-off sequence. The reduction of the lift coefficient C_L due to frost was measured using a force balance and by comparing the results with clean wing values. The upper surface boundary layer displacement thickness δ^* was measured with a boundary layer rake at the aft end of the main plane.

Before the wind tunnel run the frost thickness and geometry were determined. The average thickness was measured with an Elcometer gauge. The frost geometry was determined with two methods: laser scanning and photogrammetry. To enhance frost reflectivity in laser scanning the frost was painted with titanium dioxide. The frost surface geometry was determined with and without painting using both methods. A comparison of the results, obtained with the two methods, was performed.

II. Methodology

A. Wind Tunnel

Arteform Low Speed Wind Tunnel is a closed circuit wind tunnel with an octagonal test section with dimensions of 2 m x 2 m and a test section length of 4 m. The flow uniformity in the test section is better than 0.14 %, and turbulence level is less than 0.28 % at a constant wind tunnel speed of 60 m/s. However, during acceleration the turbulence level is somewhat higher, around 0.35 %. The turbulence level is relevant when a clean airfoil reference test is made. When the airfoil is contaminated (with frost or anti-icing fluid) it is not too sensitive for the tunnel turbulence level as the boundary layer is already much disturbed by the contamination.

The massive concrete structures of the wind tunnel ducts are outside the facility building. This makes the tunnel structure during winter time an efficient heat sink and the fan power, dissipated during a short period take-off run simulation, does not increase the test section temperature significantly (< 2 ° C). Temperatures in the test section follow roughly the daily outside air temperature (OAT). During the tests of this study the wind tunnel air temperature was around 5˚C.

There is standard measuring software in the wind tunnel collecting the wind tunnel temperature, airspeed, dynamic pressure, relative humidity, balance forces and moments (lift, drag and pitching moment) and the wing angle of attack.

B. HL-CRM Wing Model

CRM is an acronym for Common Research Model of a modern jet aircraft configuration. The generic long range twin engine configuration was first optimized for cruise flight and then high lift devices were added on the wing

defining a HL-CRM configuration, see Ref. [10].

A representative section for the present studies was selected outboard of the wing planform kink as shown in Figure 1. The section was selected in the vicinity of the wing Mean Aerodynamic Chord and is free from the local flow conditions due to the engine and wing kink. In a wind tunnel test the critical flow conditions should be reproduced. Anti-icing fluid is applied on the wing upper surface only and also the possible frost on the wing upper surface is critical due to the upper surface retarding flow at high angle of attack. For this reason the section was taken in the local upper surface stream line direction. On a wing at subsonic speeds the local streamlines are directed inboard on the upper surface and outboard on the lower surface. CFD calculations in ref. [10] showed that in take-off configuration at high angle of attack the streamlines on the wing upper surface at the station for the representative wing section were directed 11,3^{o} inboard. The wing section was taken in this direction and perpendicular to the wing plane to take into account the wing dihedral. In a low speed case even on a swept wing the flow speed and section perpendicular to the leading edge is not relevant, contrary to the situation in a high-speed subsonic case.

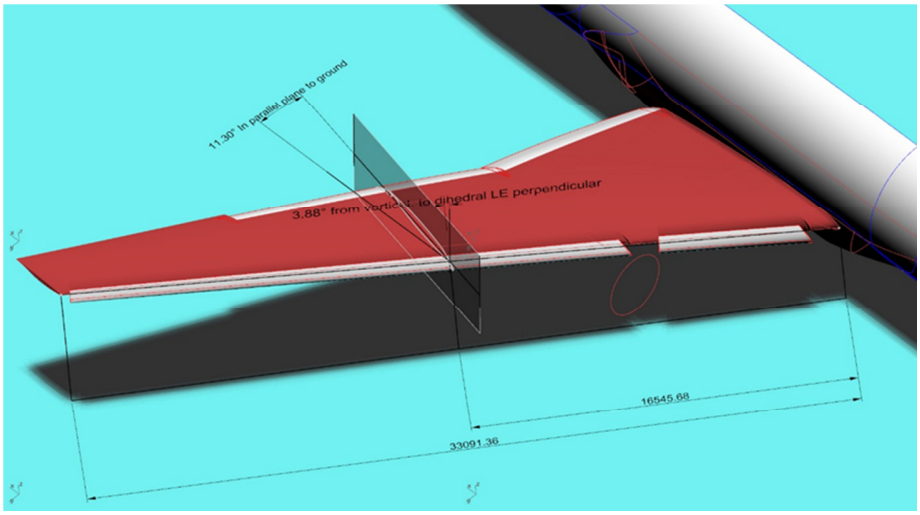

Figure 1. Wing section selection in the High-Lift Common Research Model.

For the rectangular wing model a chord of 625 mm and span of 1550 mm were chosen as a compromise of Reynolds number, test section blockage (wind tunnel corrections) and tunnel balance forces. In the tests the slat deflection was 22^{o} and the flap deflection 10^{o} to give realistic take-off conditions. The test section geometry is shown in Figure 2 and named HL-CRM Mod because the section was not taken in a wing station parallel to the aircraft symmetry plane. The HL-CRM configuration external surface was not modified. To improve the two-dimensionality of the flow end plates were designed for the model. In the tunnel test section the flow is constrained by the test section walls, floor and ceiling and the wing model lift curve slope in the linear lift range was 6,103 per radian indicating a flow close to two-dimensional.

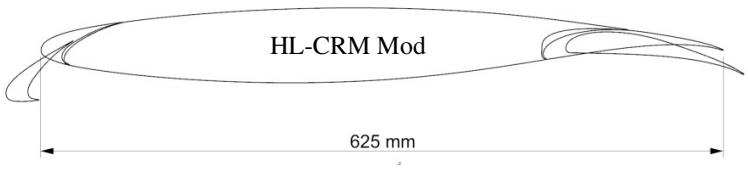

Figure 2. HL-CRM Mod wing model section with a slat deflection of 22^{o} and flap deflection of 10^{o}.

The load carrying structure of the wing model was mainly made of aerospace aluminum alloys. Bonding of parts was accomplished using epoxy adhesives. The skin thickness on the "Fuel Tank" area was 1,5 mm. The skin material was aerospace aluminum alloy. The slats and flaps were made of carbon fiber composites. The wing model with the skins, slat and flap is shown in Figure 3.

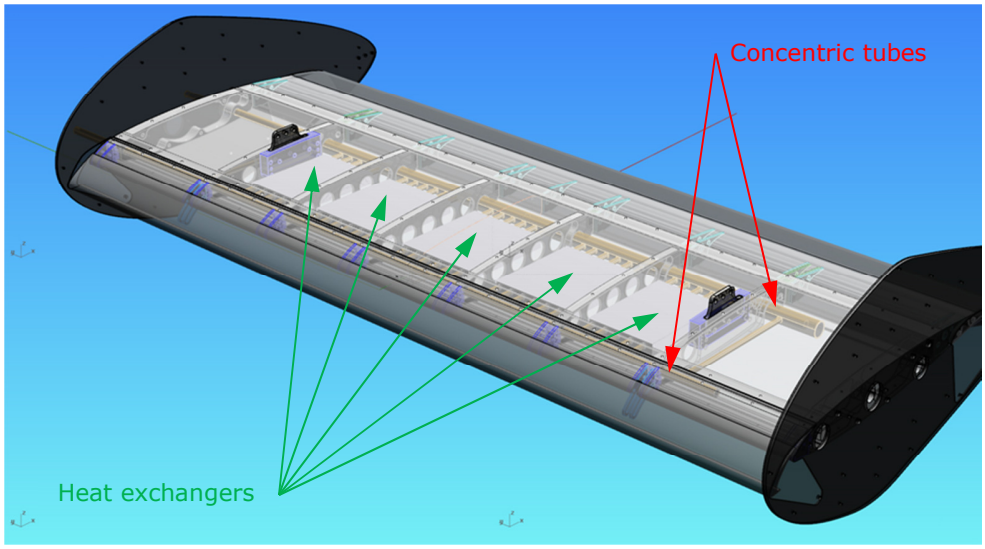

Figure 3. HL-CRM Mod wing model with end plates.

C. Frost Generation

The wing model coolant tank, which simulates an airliner fuel tank, is positioned between the dimensionless chord coordinates of x/c = 12% and 65%. Approximately 27 kg of 50/50 ethylene glycol and water mixture was used to simulate the effect of cold fuel. The tank was cooled down using a cooling circuit including heat exchangers inside the tank as shown in Figure 3. The cooling fluid was distributed to the heat exchangers via concentric tubes at the front and rear spars to enable an even temperature. The wing model temperature was monitored via several temperature sensors inside the coolant tank and on the wing skins. The cooling system was able to reach he desired wing tank temperature of -15° C to -20° C in two to three hours. The wind tunnel test section temperature was not controlled but was the same as the ambient temperature. During the winter and spring test temperatures around zero degrees Celsius were available representing airline winter operations. The created frost thickness was measured with an Elcometer thickness gauge at several points in the tank area on the upper surface of the wing. During the wind tunnel run the cooling circuit was cut off not to disturb the force balance measurements.

D. Aerodynamic Measurements

The wind tunnel measurement simulates and airliner take-off sequence which consists of three parts. First there is acceleration from standstill to the rotation speed V_R with a constant pitch attitude during the ground roll. Having reached the rotation speed the aircraft pitch attitude is increased to lift-off attitude. When airborne the speed is increased to take-off safety speed V_2 where it remains until cleaning altitude. Koivisto made in Ref. [11] an analysis with the Airbus performance software PEP on Airbus A321 take-off. The aircraft lift coefficient increased about ΔC_L=0,7…0,8 due to the rotation from the ground roll to initial climb angle of attack. The analysis also showed after rotation a lift coefficient peak due to the curved flight path. To simulate the peak in a wind tunnel test is too complicated a task and the test sequence in is a compromise. It was designed with a slat deflection 22° and flap deflection 10°. It begins with a ground roll at zero angle of attack with a lift coefficient of about C_L=0,52. The speed increases in 30 seconds to 60 m/s and is then kept constant. When reaching the 60 m/s the angle of attack is increased to 9,2° corresponding to a lift coefficient value of about C_L=1,50. The nominal rotation rate is 4,5°/s. The wing model Reynolds number at the velocity of 60 m/s is about 2,5 million.

The purpose of the aerodynamic measurements was to correlate a certain frost thickness to a corresponding lift degradation. Another goal was to correlate the lift degradation to a corresponding boundary layer displacement thickness. Both the force balance and boundary layer rake measurements were simultaneously performed as time histories during the simulated take-off sequence. The interesting part is just after the rotation.

The repeatability of the averaged lift coefficient values was within ± 0,006. The measured balance force values contain wind tunnel corrections for flow blockage due to the model and test section boundary layer but not the effect of flow curvature. Thus the accuracy is on the repeatability of the lift coefficient, not on the absolute value. When two lift coefficient values are measured it is possible that both errors have the same sign or opposite signs resulting in an error on the difference of 0 and 0,012 respectively. Or the error on the difference could be some value in

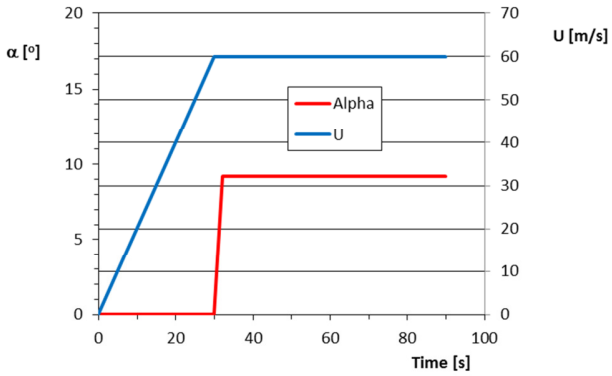

Figure 4. Variation of wind tunnel velocity U and model angle of attack α during the simulated take-off sequence.

between. Assuming that the maximum errors act simultaneously in opposite directions is probably too conservative. However, it is likely that combining two inaccurate measurements cause a larger error than in a single measurement. Often a combined error, caused by several independent factors, is estimated using a root mean square value of the individual errors. The difference of two lift coefficients will then have an inaccuracy of $\sqrt{2}$ *0,006 =0,0085.

The lift reduction due to frost was determined by estimating the average lift coefficient after the rotation with and without frost on the wing. The results are presented as relative lift degradation $\Delta C_L/C_{LClean}$ as function of dimensionless frost thickness t/c as a dimensionless presentation permits direct comparison with different airfoils and wings. The absolute reduction of the two-dimensional lift coefficient is transformed into wing lift coefficient reduction in the linear range in proportion of the three and two-dimensional lift curve slopes. Consequently the absolute value of the wing lift coefficient reduction is lower than on the two-dimensional airfoil, but the relative reductions are the same. As the selected wing section for the wind tunnel model is representative for the HL-CRM jet aircraft configuration also the lift reduction is representative for the configuration.

The boundary layer displacement thickness values, corresponding to the lift force measurements, were measured with a boundary layer rake at the aft edge of the airfoil main element. Two different surface conditions in the same test case could be measured with two rakes simultaneously. The rake setup is shown in Figure 5. The accuracy of the displacement thickness measurements was ± 0,32 mm. When calculating the difference of two boundary layer displacement thicknesses the accuracy is reduced to $\Delta\delta^* = \sqrt{2}$ *0,32=0,46 mm.

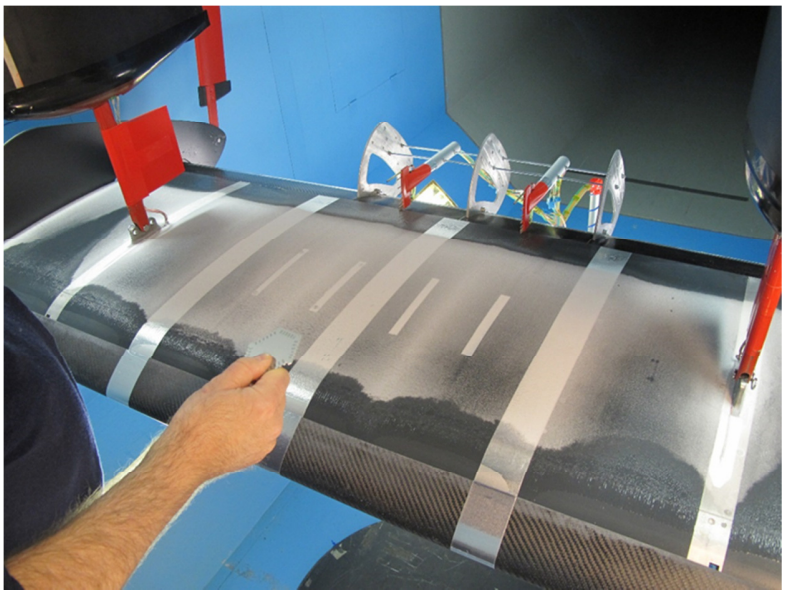

Figure 5. The double rake set up on the wing model.

E. Laser Scanning

Laser scanning of the frost geometry was performed for two reasons. First the lift degradation in the wind tunnel test needs to be related to a frost thickness. The second goal was to compare laser scanning with photogrammetry as a method for frost geometry determination.

Laser scanning of the frost was performed with a Romer Absolute Arm 7530SI laser imaging equipment. Scans were performed on the clean wing surface without frost, on the frosted surface and, to enhance the reflectivity of the frost surface, also on a painted frost surface. The scan of the clean wing test square was performed at cold temperature corresponding to the frost test condition. To align the scanner with the model there were four conical contact points on the wing model, see Figure 6. The scanning test square was marked with tape. NASA "ice accretion paint" with titanium dioxide was applied to frost surface in the scanning area using an automotive-style spray gun. The scanning was performed manually by moving the scanner head over the test square in two perpendicular directions. When scanning the unpainted frost the scanning parameters were tuned by arranging a similar lighting on a white paper and locking the exposure setting for use on frost scanning. The scanning operation took about 10 minutes and was done before the wind tunnel test run so that the initial frost geometry before the take-off was known. Dismantling the laser equipment took about 10 minutes.

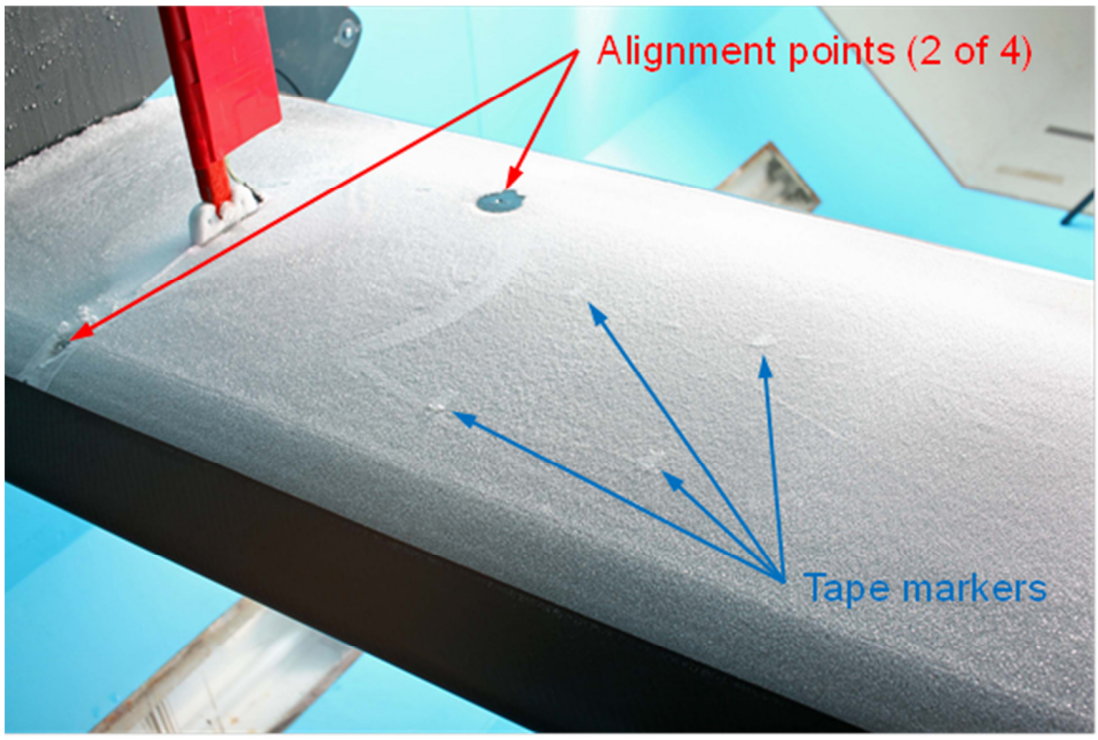

Figure 6. Wing model alignment points and tape markings of the test square.

F. Photogrammetry

Photogrammetry had the same two goals as laser scanning, namely frost thickness measurement and frost surface geometry determination. The wing was imaged in three different conditions, clean wing, frosted wing and painted frosted wing. Each imaging process was carried out with a similar process which consisted of three imaging lines, one vertical line and two oblique lines as illustrated in Figure 7. Nikon D810 camera equipped with Sigma ART 85mm f1.4 lens was used throughout the imaging process. The camera was placed on top of the wing by securely mounting it to a plywood plate. The camera shutter was operated with wireless remote controller to avoid unnecessary disturbances that may cause camera movement during the image capture. Due to the provisional camera setup and usage of only one camera it had to be moved between the three positions. Moving the camera and taking several photographs in each position lead to a photogrammetry operation of about half an hour to one hour. The camera setup was however not stiff enough and only one photograph from each position could be utilized in the analysis. Having a good camera fixture with three cameras would enable an operation time of less than 5 minutes, improvement in accuracy with several pictures from one position and also photographing during a tunnel run.

Figure 7. The wing model and the structure of image block

The bundle block adjustment and the dense point cloud calculation were carried out with Pix4DmapperPro 3.2.23 software. Full image resolution was used in "Find Keypoints" step and Aerial Grid or Corridor method with "Use Geometrically Verified Matching enabled" were used for pair matching. Moreover, all inner camera calibration parameters were solved during the bundle block adjustment. The dense point cloud calculation was done with full resolution Image Scale and Point Density was set to Optimal. Minimum number of Matches was set to 3 and Matching Window Size was set to 7x7.

The scale for the photogrammetric block was determined during the bundle block adjustment. Therefore, a known object was placed on the imaging area. The object to be used was an Elcometer disc that was calibrated in the Finnish Geospatial Research Institute's calibration laboratory by horizontal comparator. Figure 8 shows the test square marked in red and the Elcometer disc beside the area. The entire photograph in the figure is the size of the photograph used in photogrammetry. 3DReshaper was used to align photogrammetric point clouds with the laser data to the same coordinate system. 3DReshapers Best align N points tool was used with four common points. Washers were used for the four alignment points and they are visible in the figure at the corners of the red square.

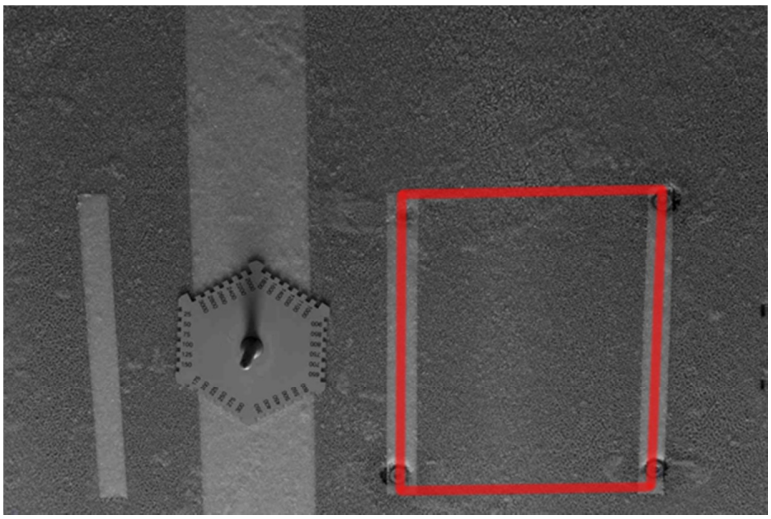

Figure 8. The Elcometer disc and the test square.

G. Test Procedure

As the laser scanning, photogrammetry and aerodynamic wind tunnel test were performed for a certain frost geometry, the measurements had to be performed in a certain order. The testing process was started with frost creation during which the wing tank and skin temperatures were registered. Also the test section air temperature and relative humidity were registered.

After frost creation followed frost thickness measurements with Elcometer gauge. Frost thickness was measured in nine locations around the test square. An average value and standard deviation was calculated from the measured values. Laser scanning and photogrammetry was then performed on the right hand side test square frost without painting. The right hand side test square was painted with titanium oxide and then again imaged with laser and photogrammetry. A wind tunnel run was performed simulating an aircraft take-off sequence. During the run the wing lift coefficient was measured. The boundary layer displacement thickness was simultaneously measured on the painted frost surface on the right hand side and the unpainted frost on the left hand side.

When the frost had disappeared the clean wing surface was measured in cold condition as a reference with laser imaging and photogrammetry. By positioning the clean wing surface in relation to the frost surface the frost thickness could be calculated. Finally a wind tunnel run was made simulating the aircraft take-off sequence. The clean wing lift coefficient and boundary layer displacement thicknesses on the left and right hand sides were measured as a reference.

III. Results and Discussion

A. Laser Scanning and Photogrammetry

The quality of laser scanning was evaluated by using thickness and point densities of the frosted layers. Frost thickness was calculated by comparing the clean wing surface with the frosted ones. Two different methods for thickness determination were used. The first was a cross section of the point clouds. The second method was to calculate a difference surface between the clean wing surface and the frosted ones. The clean surface was kept as a reference.

Comparisons of the cross section of the point clouds, measured with laser scanning and photogrammetry, are presented for unpainted and painted frost in Figure 9. On unpainted frost the cross section thickness, derived with laser scanning, was noticeably smaller than the one derived with photogrammetry. On the painted frost photogrammetry gave only a slightly larger thickness than laser scanning.

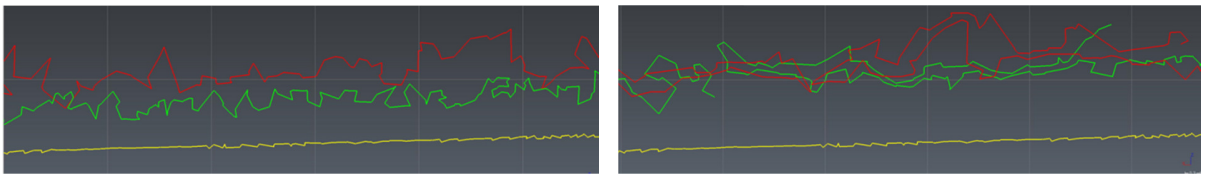

(a) unpainted frost (b) painted frost

Figure 9. A close up view of the point cloud cross sections. The laser scanned section is in green, the photogrammetric section in red and the clean wing surface in yellow color. The grid scale is 2 mm.

Figure 10 (a) and (b) show the unpainted and painted frost thickness surfaces, derived by laser scanning, with the average thickness indicated on the right hand side scales. The measured average thickness was increased from 0.8 mm to 1.3 mm after applying a paint layer on top of the frost. Figure 11 (a) and (b) show the photogrammetry results on the unpainted and painted frost thickness surfaces. It can be noted that there is a slight increase in in the average frost thickness between the unpainted and painted frost thicknesses. The average thickness for the unpainted frost was 1.3 mm, which was increased to 1.5 mm due to the painting. The thickness measurement with the Elcometer gauge gave for the unpainted frost an average thickness of 1.343 mm with a standard deviation of 0.184 mm. A possible explanation for the considerably smaller thickness, derived by laser scanning, is that the laser signal may have penetrated into the frost due to the low reflectivity. The individual Elcometer measurements tend to give a thickness value in the vicinity of the local maximum frost thickness as the tool is a mechanical gauge.

The resolution in point position measurements by photogrammetry was assessed as 0.05 mm. In laser imaging the resolution on clean wing surface point position was 0.03 mm, but due to the lower frost reflectivity the resolution was reduced to about 0.50 mm on unpainted frost. Painting the frost improved the surface reflectivity, but the added thickness reduced the resolution to about 0.23 mm. It seems that photogrammetry gives more reliable results on frost thickness than laser scanning. Painting the frost before imaging feels a possible source of errors besides the added

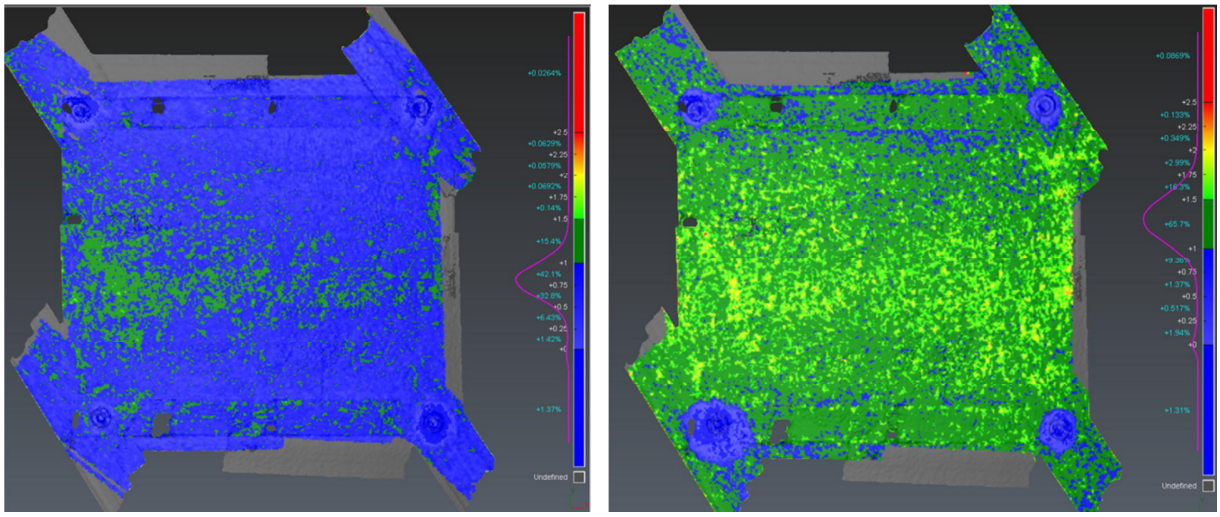

(a) unpainted frost (b) painted frost

Figure 10. Thickness of the frost measured with laser scanning.

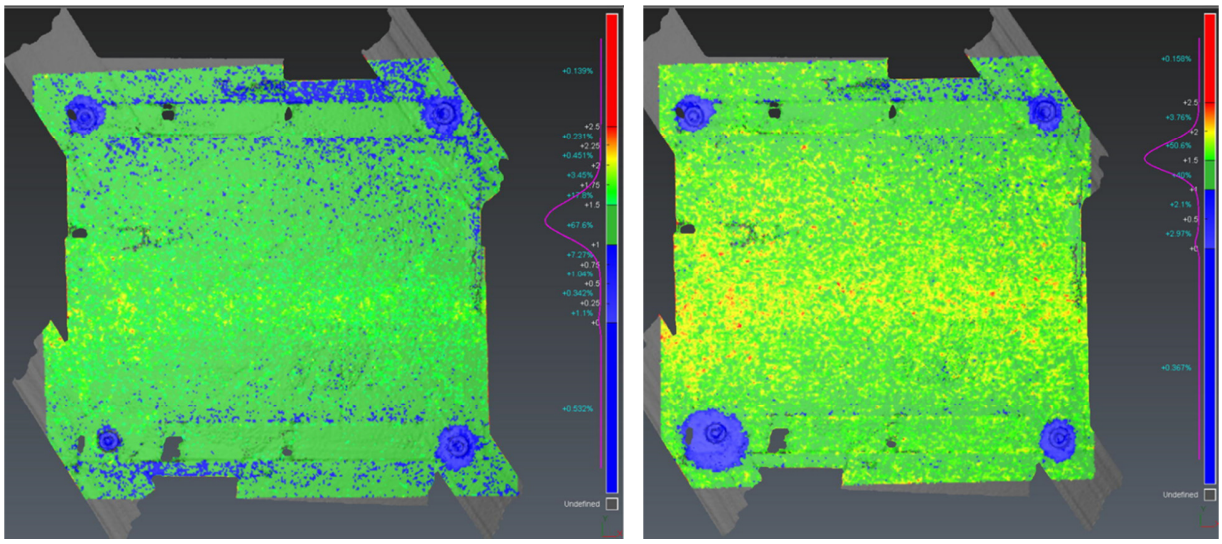

(a) unpainted frost (b) painted frost

Figure 11. Thickness of the frost measured with photogrammetry.

thickness as the paint may fracture or melt the frost crystals and fill the space in between and on top of the crystals.

For the unpainted frost the point densities were 530 and 375 points per mm^2 for laser scanning and photogrammetry respectively. With evenly spaced points 400 point per mm^2 implies a distance between the closest two points of 0.05 mm.

B. Lift Degradation and Boundary Layer Displacement Thickness

Both the force balance and boundary layer rake measurements were simultaneously performed as time histories during the simulated take-off sequence. Depending on the conditions during the wind tunnel run the frost melted/sublimated/detached off the wing surface, see Fig. 12. This manifested in a changing lift force and boundary layer displacement thickness. The interesting part is after the rotation during the take-off. It was also intended to measure the effect of painting the frost on the displacement thickness. However, due to a misunderstanding only the test square was painted and the effect of that was due to the limited area rather small.

The lift reduction due to frost was determined in the above mentioned figures by estimating the average lift

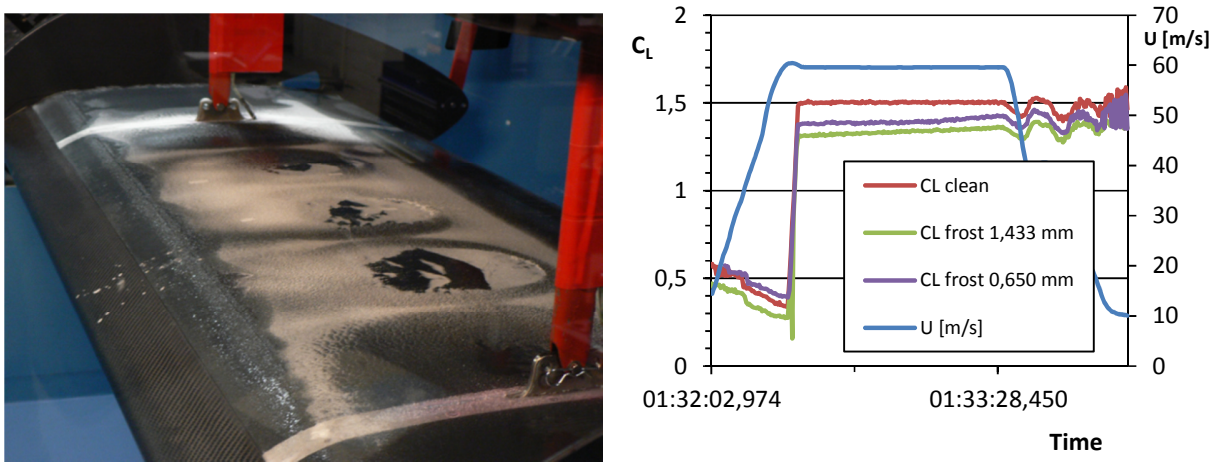

(a) frost melting, evaporation and detachment (b) measurement time history

Figure 12. Frost and lift coefficient behavior during a simulated take-off sequence wind tunnel run.

coefficient after the rotation with and without frost on the wing. The relative lift degradation $\Delta C_L/C_{LClean}$ as function of dimensionless frost thickness t/c is presented in Figure 13. The present measurements of Ref. [12] are presented together with earlier measurements on HL-CRM Mod and DLR-F15 airfoils and show fairly linear characteristics. The relative degradations are only slightly different for the two airfoils at the different ambient temperatures and tend towards zero with diminishing frost thickness. There was no melting or detaching of the frost noticed during the take-off roll in these cases.

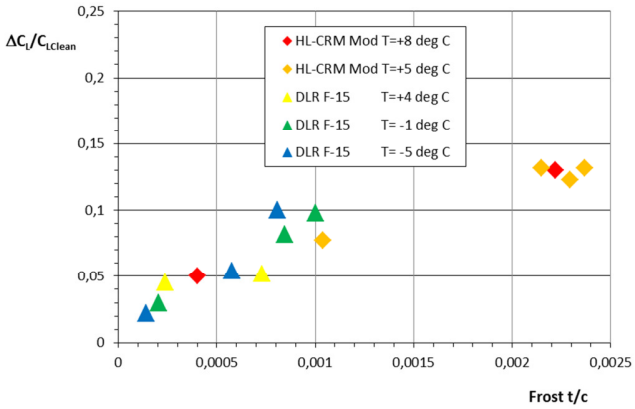

Figure 13. Relative lift coefficient degradation $\Delta C_L/C_{Lclean}$ as function of dimensionless frost thickness t/c measured on HL-CRM Mod and DLR-F15 wing models at different ambient temperatures.

Because the relative lift degradation, which is independent of the model wing aspect ratio, is a directly indicative entity it can be compared with the limit value of 5,24 % that has been used as an acceptance limit for anti-icing fluid effect, see Hill & Zierten Ref. [13] and Broeren & Riley Ref. [14]. Using this limit value Figure 13 indicates an allowable dimensionless frost thickness in the order of t/c=0.0005 when the temperature is so low that there is no noticeable evaporation/melting/detaching of the frost during the take-off roll. This is only an indication however, as Broeren & Riley in Ref. [14] point out, that the trends on percentage lift losses in two-dimensional flow at linear lift range and three-dimensional flow at maximum lift may be different. Another reason for inaccuracy in lift coefficient reduction is the Reynolds number in the present tests, which was lower than for a full scale aircraft in take-off situation. The allowable frost thickness should be confirmed with three-dimensional wind tunnel or flight testing for the aircraft configuration in question.

The boundary layer displacement thickness values, corresponding to the lift force measurements, were measured as time histories. The measurement interval was 0.02 seconds, but moving average was calculated to smooth out the

results. In spite of this the time histories showed quite detailed characteristics, see Figure 14. Examples of boundary layer velocity profiles just after rotation are show in the same figure. The displacement thickness values can be correlated to the respective frost thicknesses. Consequently it is possible to relate a lift reduction to boundary layer growth. The relative lift degradation due to frost is presented as function of dimensionless boundary layer growth in Figure 15. As is seen in the figure the lift degradation is fairly linear with increasing displacement thickness and tends to zero with zero displacement thickness chance.

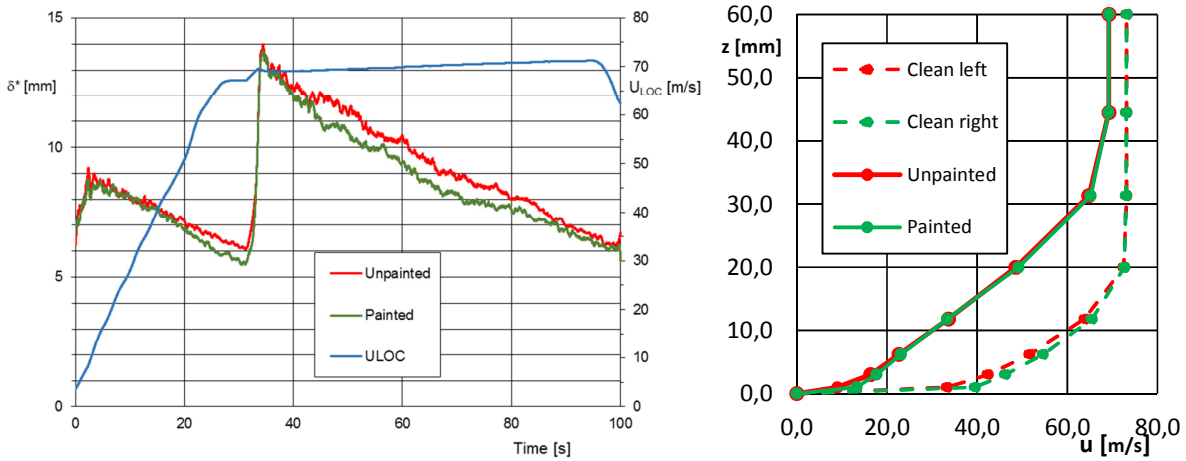

(a) Displacement thickness time history (b) Velocity profiles after rotation

Figure 14. Boundary layer behavior during a simulated take-off on a wing with painted and 1,343 mm of unpainted frost. The blue line shows the tunnel flow speed.

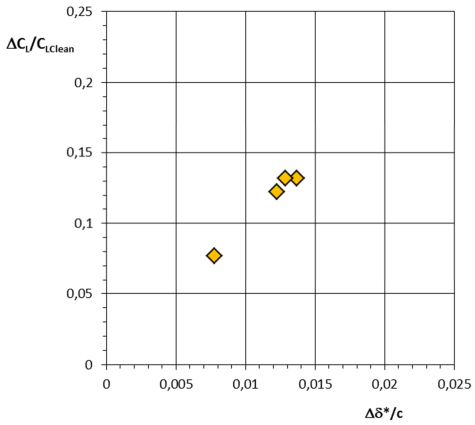

Figure 15. Relative lift coefficient degradation $\Delta C_L / C_{LClean}$ as function of dimensionless displacement thickness change $\Delta\delta^*/c$.

IV. Conclusions

The test campaign showed, that laser scanning the frost, without first painting it, is possible by tuning the exposure. Laser scanning however gave for the unpainted frost an average thickness of 0.8 mm whereas photogrammetry gave an average value of 1.3 mm. The latter matches fairly well the average value of 1.343 mm, calculated from the Elcometer thickness gauge measurements. A possible explanation for the difference is that the laser signal may have penetrated into the unpainted frost.

On painted frost laser scanning gave an average thickness of 1.3 mm and photogrammetry an average value of 1.5 mm. It feels plausible that painting has increased the measured thickness. Painting feels a complication as it may

fracture or melt the frost crystals and fill the cavities in between. For this reason geometry measurements without painting may have an advantage.

The aerodynamic measurements showed that the effect of frost, compared with a clean wing, had a measurable effect on the lift coefficient and boundary layer displacement thickness. A dimensionless frost thickness of t/c=0.0005 gave a relative lift coefficient degradation of about $\Delta C_L/C_{LClean}=0.05$. This is about the same as the 5.24 % reduction, which is generally accepted in take-off with anti-icing fluids.

Acknowledgments

The laser scanning and wind tunnel measurements were performed by Arteform Ltd. The photogrammetry measurements and post processing of laser scanned and photogrammetry data was performed by National Land Survey of Finland. Support from the U.S. Federal Aviation Administration and Finnish Transport Safety Agency is gratefully acknowledged.

References

[1] Koivisto P., A Literature Review on Cold Soaked Fuel Frost Formation and Sublimation, Finnish Transport Safety Agency, Trafi Research Reports 6-2015, Helsinki, Finland, 2015. https://www.trafi.fi/en/aviation/aviation_and_the_environment/icewing_-_research_on_aircraft_wing_de_anti-icing_fluids

[2] Ljungström B.L.G., Windtunnel investigation of simulated hoar frost on a two-dimensional wing section with an without high lift devices, Report FFA-AU-902, Stockholm, Sweden, April 1972.

[3] Oolbekkink B., Volkers D.F., Aerodynamic Effects of Distributed Roughness on a NACA 632-015 Airfoil, AIAA Paper 91-0443, 1991.

[4] Kind R.J., Lawrysyn M.A., Aerodynamic Characteristics of Hoar Frost Roughness, AIAA Journal, Vol. 30, No. 7, July 1992.

[5] Bragg M.B., Heinrich D.C., Valarezo W.O, McGhee R.J., Effect of Underwing Frost on a Transport Aircraft Airfoil at Flight Reynolds Number, Journal of Aircraft Vol. 31, No. 6, 1994, pp. 1372, 1379.

[6] Koivisto P., Effects of Cold Soaked Fuel Frost on Lift Degradation during Simulated Take-off, Finnish Transport Safety Agency, Trafi Research Reports 4-2015, 2015, 24 p.

[7] Koivisto P., Preliminary Cold Soaked Fuel Frost Studies with CRM Wing Model, Finnish Transport Safety Agency, Trafi Research Reports 12-2016, Helsinki, Finland, 2016, 11 p.

[8] Code of Federal Regulations, Title 14 Aeronautics and Space, Volume 3, Chapter I, Subchapter G, Part 121, Federal Aviation Authority, Department of Transportation, Operating Requirements, Domestic, Flag, and Supplemental Operations, August 25, 2017.

[9] Commission Regulation (EU) No 965/2012, 5 October 2012, 148 p.

[10] Lacy D.S., Sclafani A.J., Development of the High Lift Common Research Model (HL-CRM): A Representative High Lift Configuration for Transonic Transports, AIAA Paper 2016-0308, 24 p.

[11] Koivisto P., Effects of Anti-icing Treatment on Lift Degradation during Simulated Take-off, Finnish Transport Safety Agency, Trafi Publications 25-2103, Helsinki, Finland, 2013, 22 p.

[12] Soinne E., Rosnell T., Viljanen N., Aerodynamic, Laser and Photogrammetry Measurements on CRM Wing Model with Frost, Finnish Transport Safety Agency, Trafi Research Reports 11-2017, Helsinki, Finland, 2017, 60 p.

[13] Hill E.G., Zierten T.A., Aerodynamic Effects of Aircraft Ground Deicing/Anti-Icing Fluids, Journal of Aircraft, Vol. 30, No.1 Jan-Feb 1993, page 24-34.

[14] Broeren A.P., Riley J.T., Review of the Aerodynamic Acceptance Test and Application to Anti-Icing Fluids Testing in the NRC Propulsion and Icing Wind Tunnel, NASA/TM-2012-216014, 2012, 34 p.